

S986 in M67: A Totally-Eclipsing Binary at the Cluster Turnoff

Eric L. Sandquist

San Diego State University, Department of Astronomy, San Diego, CA 92182

erics@mintaka.sdsu.edu

Matthew D. Shetrone

University of Texas/McDonald Observatory, P.O. Box 1337, Fort Davis, Texas 79734

shetrone@astro.as.utexas.edu

ABSTRACT

We have discovered that the star S986 in the old open cluster M67 has detectable total eclipses of depth 0.08 mag for the primary eclipse and 0.011 mag for the secondary eclipse (in I only). We confirm the detection of a third star in spectra contributing $(11.5 \pm 1.5)\%$ of the total light in V band. The radial velocity of the third star indicates that it is a cluster member, but it is unclear whether it is physically associated with the eclipsing binary. Using spectroscopic and photometric data, we deconvolve the photometry of the three stars, and find that the primary star in the eclipsing binary is significantly hotter than the turnoff. The two most likely explanations are that the primary star is in a rapid phase of evolution near core hydrogen exhaustion (associated with the turnoff gap in M67's color-magnitude diagram), or that it is a blue straggler created during a stellar collision earlier in the cluster's history. Our detection of Li in the primary star tightly constrains possible formation mechanisms in the blue straggler explanation. Because S986 is often used to constrain tidal dissipation models, this may imply that the strength of tidal effects is underestimated.

Subject headings: open clusters: individual (NGC2682) — stars: individual (S986) — binaries: eclipsing — blue stragglers

1. Introduction

M67 is probably the most thoroughly studied old open cluster in the Galaxy, thanks to its small distance from us. Typically quoted values for the cluster's age (4 ± 0.5 Gyr; Dinescu et

al. 1995) place it between the majority of known open clusters and the much older globular clusters. A determination of the mass of turnoff stars in this cluster would immediately provide us with a means of critically testing the validity of theoretical stellar evolution tracks, and checking models of various physical effects (such as convective overshooting and chemical diffusion). However, because M67 seems to have a high binary star fraction ($\sim 50\%$; Fan et al. 1996) and there is definite evidence of strong dynamical interactions among cluster members (e.g. van den Berg et al. 2001; Sandquist et al. 2003), special care must be taken to ensure that the stars in such a binary have not been influenced by their environment.

Accurate photometry of the star S986 [ID number from Sanders 1977; also known as F111 (Fagerholm 1906), and MMJ 5624 (Montgomery, Marschall, & Janes 1993)] indicates that it falls at the turnoff in the cluster’s color-magnitude diagram (CMD), and proper motion studies identify it as a high probability ($\geq 95\%$) member of the cluster (Sanders 1977; Girard et al. 1989; Zhao et al. 1993). S986 was previously identified as a single-lined spectroscopic binary by Mathieu, Latham, & Griffin (1990) with a period $P = 10.3386 \pm 0.0006$ d. Another interesting aspect of this system is the fact that the primary is on a circular orbit, indicating that tidal interactions between the stars have damped out any initial eccentricity. Over time, circularized main sequence binaries should be found at longer and longer periods as these interactions have sufficient time to work in wider and wider binaries (Mathieu & Mazeh 1988). S986 is the longest period circularized binary known in the cluster, and has probably required most of the cluster’s lifetime to become circularized.

As Mathieu et al. (1990) discuss, the secondary star in the binary must be at least about 2 magnitudes fainter than the primary at 5200 \AA because it is a single-lined system. This indicates that the primary must contribute most of the light coming from the system, and therefore must be very close to the turnoff mass. A lower limit on the mass of the secondary is placed by the mass function for the binary: approximately $0.51 M_{\odot}$ in the case of S986 (assuming a primary mass of $1.25 M_{\odot}$). Mathieu et al. stated that residuals of the orbital solution correlated with phase, and that a weak secondary cross correlation peak could be seen. Later Melo, Pasquini, & De Medeiros (2001) definitively detected a secondary peak in the cross-correlation function for the system, and measured a rotational velocity $v \sin i = 5.3 \pm 0.6 \text{ km s}^{-1}$. Careful examination of their cross correlation function indicates that the secondary peak is rather close to systematic radial velocity for M67.

As a byproduct of our project to monitor the partially-eclipsing blue straggler S1082 (period 1.0677978 d), we made extensive observations of the fields near the core of M67. The period of S986 has unfortunate aliases with the period of Earth’s rotation so that only one good apparition of the primary eclipse occurs during nighttime hours for a given observing site per month. This may explain the reason that eclipses have not previously been detected

for this system. In the following sections, we describe our spectroscopic and photometric observations and reduction, the modeling of the light curve, and finally a discussion of the astrophysical meaning.

2. Spectroscopic Observations and Reduction

Because the spectroscopic observations of S986 provide very important constraints on the properties of the stars involved, we discuss them first. Our spectra were obtained at the Hobby-Eberly Telescope (HET) with the High Resolution Spectrograph (HRS) as part of normal queue scheduled observing for the period 2003-1. Our initial spectra were taken with the purpose of investigating the detection of a secondary peak in the cross-correlation function (CCF) by Melo et al. (2001). The spectra were taken with the three arcsecond science fiber with one sky fiber at 60,000 resolution. Exposure times were 540 seconds and yielded signal-to-noise (S/N) of 28 per resolution element. Follow-up spectra were taken with the two arcsecond science fiber with two sky fibers at 15,000 resolution. Exposure times were 1000 seconds and yielded S/N of 100 per resolution element. The spectra were reduced with IRAF¹ ECHELLE scripts.

To determine radial velocities, we employed the IRAF task FXCOR to cross-correlate the reduced spectra against a solar spectrum taken with the same spectrograph. We confirmed the secondary peak in the CCF, and deblended the two components using Gaussian profiles with independent centroids and FWHM. The region used for determining the CCF was 5420 - 5720 Å for the 60,000 resolution spectra and 5960 - 6440 Å for the 15,000 resolution spectra. We find no discernible radial velocity variation of the secondary peak even though we observed the primary star at its maximum deviation from the cluster mean, and so we conclude that it is not the secondary component of the binary. Although we did examine the CCF for an even fainter third component, we did not find any significant traces. The secondary peak in the CCF sits at the cluster velocity (33.5 km s⁻¹; Mathieu & Latham 1986), so that we conclude it is a cluster member: either a chance superposition or a third star on a wide orbit around the inner binary. We will denote the bright star in the binary as component Aa, and the third star as component B. The velocities measured for these two components are given in Table 1. The FWHM for the primary component Aa was found to be consistent with no detectable rotation (< 10 km s⁻¹) given our resolution, while the

¹IRAF (Image Reduction and Analysis Facility) is distributed by the National Optical Astronomy Observatories, which are operated by the Association of Universities for Research in Astronomy, Inc., under contract with the National Science Foundation.

tertiary component B was found to have a small detectable rotational broadening (12 ± 4 km s⁻¹).

The 60,000 resolution spectra were then shifted to the zero velocity for component Aa and combined to produce a higher S/N master spectrum that was used for an abundance analysis. The techniques employed here are nearly the same as those used in Shetrone & Sandquist (2000): equivalent widths were measured and abundances computed for each line. The temperature, surface gravity, and microturbulence were varied to minimize the slopes in the abundance vs. excitation potential and abundance vs. reduced equivalent width plots, and also to force ionization equilibrium. As an additional constraint, we limit the microturbulence to a value consistent with the formula given by Edvardsson et al. (1993) as a function of surface gravity and effective temperature to within their quoted errors (0.3 km s⁻¹). One departure from the analysis of Shetrone & Sandquist (2000) was the use of a flux contribution variable that was divided into Aa’s EW to compensate for the contribution of the B spectral component (although the B component’s spectral lines were removed the flux contribution remains in our master Aa spectrum). The flux contribution variable was set by forcing the overall derived metallicity to be the same as the cluster mean (-0.05 ; Shetrone & Sandquist 2000). Using this technique we found the primary component has a $T_{eff} = 6400 \pm 50$ K, $\log g = 4.25 \pm 0.08$, $v_t = 2.0 \pm 0.1$ km s⁻¹ and a flux contribution of 0.885 ± 0.015 . Because the “third light” contribution to the system flux by component B affects the observed depths of the eclipses described below, this measurement is an important ingredient in determining system parameters.

As part of the abundance analysis we detected a small Li line in the master spectrum of the Aa component having an equivalent width of 10 mÅ. This corresponds to $\log N(Li) = 2.11^{+0.2}_{-0.4}$ (see Fig.1), which is near the lower limit of 2.04 derived by Jones, Fischer, & Soderblom (1999) from data from García López, Rebolo, & Beckman (1988) (although without any corrections for the other components). In addition, our examination of O, s-process, and α elements for component Aa seem to be normal for main sequence or blue straggler stars (Shetrone & Sandquist 2000).

A master B spectrum was created by dividing the master Aa component into the individual spectra and then shifting the spectra to the rest velocity of the B component and combining. Unfortunately, because of the low S/N of the R=60,000 spectra, individual EW could not be measured from that master B spectrum, although the R=15,000 spectra had sufficient signal to identify the weak B component lines (typical EW = 8 mÅ). An abundance analysis technique similar to the one described above was applied to this B component but due to the small number of lines and high noise, we were forced to constrain the surface gravity using the assumption that the B component is a main sequence dwarf with a surface

gravity and microturbulence appropriate to its T_{eff} . Using this technique we find that the B component has $T_{eff} = 5750 \pm 200$ K with a flux contribution of 0.097 ± 0.025 .

3. Photometric Observations and Reductions

All of the photometry for this study was taken at the 1 m telescope at the Mt. Laguna Observatory using a 2048×2048 CCD on nights between December 2000 and November 2002. The nights of observations are given in Table 2. The photometry was in V and I bands with typical exposure times of 20 s (ranging between 15 and 60 s). Exposures were usually separated by about 2.5 minutes due to a relatively long readout time for the CCD.

Most of the details of the reduction are presented in other papers (Sandquist et al. 2003, Sandquist & Shetrone 2003), so we only briefly describe the reduction here. The object frames were reduced using overscan subtraction, bias frames, and flat fields. We conducted aperture photometry using the IRAF tasks DAOFIND and PHOT from the AP-PHOT package. In order to improve the accuracy of the relative photometry for the light curves, we used an ensemble photometry method similar to that described by Honeycutt (1992), iterating toward a consistent solution for photometric zeropoints for all frames and average magnitudes for all stars. Because frames typically had more than 300 measurable stars, the formal errors in the zero points ranged from around 0.003 to 0.007 mag, even with respect to night-to-night variations. Our V and I data (given relative to the median magnitude) are presented in Tables 3 and 4, respectively.

Our photometry has been calibrated using cluster frames taken during the same photometric night as a large number of Landolt (1992) and Stetson (2000) standard stars. We leave the details of the calibration and the comparison with previous datasets to a separate paper (Sandquist 2003).

4. Light Curves

Using our observations, we first updated the ephemeris of Mathieu et al. (1990). We have four sequences of photometric observations covering the ingress to primary eclipse, and one set of observations covering a portion of an egress. Because the system appears to be non-interacting, it is reasonable to expect that the period of the system has remained constant since the radial velocity observations tabulated by Mathieu et al. (1990). Times of eclipse contacts were determined by χ^2 minimization for the light curves relative to a trial model light curve. The times of observed first contact were HJD 2451959.83, 2452352.68,

2452383.69, and 2452662.83, while a fourth contact was observed at HJD 2452228.95, and one mid-eclipse point could be determined at HJD 2452600.96. This information was used in a simultaneous five-parameter fit to the combined dataset, where the parameters used were period P , epoch of primary eclipse T_0 , system velocity γ , velocity semi-amplitude K_1 , and phase half-width of primary eclipse $\delta\phi_p$, assuming that the orbit has zero eccentricity. (Tests indicated that there was no measurable eccentricity.) The ephemeris for primary eclipse is

$$2445788.13(1) + 10.33813(7) \cdot E$$

The numbers in parentheses indicate the uncertainty in the last digits of T_0 and P . The period is consistent (as expected) with the value of Mathieu et al. to within their quoted error. The velocity parameters also match the Mathieu et al. measurements very well since the same radial velocity data was used: $\gamma = 33.7 \pm 0.1 \text{ km s}^{-1}$ and $K_1 = 33.8 \pm 0.2 \text{ km s}^{-1}$. Finally, the fit constrains the width of primary eclipse to be $\phi_4 - \phi_1 = 2\delta\phi_p = 0.0318 \pm 0.0084$. The reduced χ^2 for the overall fit was 1.32.

Phased data for the phases of primary and secondary eclipse are shown in Figs. 2, 3, and 4. The curvature of the light curve at second and third contacts (entering and exiting total eclipse) indicates that the primary eclipse is indeed due to a smaller star transiting across the face of a larger star.

4.1. Eclipse Depths

The eclipse depths provide robust information about the flux ratios of the two stars (although this is affected by the third star contributing to the system’s light). The overall depth of the primary eclipse is approximately 0.086 mag in V and 0.078 mag in I , consistent with eclipse by a faint cool companion. The secondary eclipse was not detected in V , but we did find evidence of a decrease in brightness in I on several nights. Data taken on the night with best atmospheric conditions (Jan. 17/18, 2003) provided our cleanest measurement of the depth of the secondary eclipse in I (0.0111 ± 0.0011 mag) using the difference between the average magnitudes out of eclipse and in total eclipse. (It appears that there was a slight zero-point differences between the two nights, so a single reference level in I was not used. This may have come about because the majority of our measurements in I were taken during nights of eclipse.) We have a second measurement of the eclipse depth (0.0101 ± 0.0013 mag) from Apr. 20/21, 2003. Combining these measurements, we have a final value 0.0107 ± 0.0008 mag.

4.2. Inclination and Radius Ratio

The ratio of the radii of the two stars is also a robust measurement because it depends on the timing of inner and outer contacts. Even with an uncertain contribution from third light, the radii of the two stars as determined from models are correlated, which means that the radius ratio is minimally affected. With fairly high time resolution observations, the times of contact can be measured directly. However, due to the duration of the eclipses, we have not yet been able to observe more than two eclipse contacts per night, so that some light-curve modeling is necessary. The phase width of the primary eclipse primarily constrains the inclination of the system and the sizes of the two stars relative to the orbital separation. Though we do not have a radial velocity curve for the secondary star, the resultant uncertainties in the mass ratio q do not significantly affect the light curve fit. Because the secondary star acts like an almost perfectly black circular mask for most of the purposes of the modeling the primary eclipses, uncertainties introduced by error in the effective temperatures of the components are also minimal.

We have used the program NIGHTFALL², which allows the use of model atmospheres (Hauschildt et al. 1999) and the modeling of physical effects such as detailed reflection. Detailed fitting of the primary eclipse requires some care in choosing the limb-darkening law. We have chosen to use a two-parameter square-root law based on literature comparisons with model atmospheres (Van Hamme 1993; Díaz-Cordovés, Claret, & Giménez 1995). Trials indicate that there are no observable indications of ellipsoidal shapes for the components, or significant reflection effects.

We computed light curve models covering a grid in the flux fraction of the primary $f_{Aa}(V)$, and the inclination of the binary I . We have imposed a constraint that the star contributing the third light should be on the single star fiducial line for M67. This assumption is not important for the determination of the inclination, but it has a slight effect on the radius determinations, especially if the star is itself an unresolved binary.

Although the uncertainty in the third light contribution has a significant effect on the uncertainties in the stellar radii, the uncertainty in the inclination dominates. The stellar radii are correlated with the inclination, with smaller inclinations requiring larger stellar radii to maintain the totality of the eclipse. Based on χ^2 minimization, the inclination is 89^{+1}_{-3} where the lower limit is set by when the primary eclipse unavoidably becomes partial. A more stringent lower limit can be derived based on when differences between observations and

²See <http://www.lsw.uni-heidelberg.de/~rwichman/Nightfall.html> for the program and a user manual (Wichmann 1998)

the best-fit model become significant at the 3σ level. Based on this we quote an inclination $i = 89^{+1}_{-2}$. In Figs. 2 and 3, we compare our data with best fit models of two different inclinations. The model fits at lower inclination first begin to become unsatisfactory at the contact points ($\phi \approx \pm 0.015$ and ± 0.01). Using this constraint, the ratio of the stellar radii is $R_{Ab}/R_{Aa} = 0.268^{+0.015}_{-0.004}$, where the uncertainties include the uncertainty in $f_{Aa}(V)$.

4.3. Photometry of the Primary Star and its Identity

The measured T_{eff} and flux contribution from component B (providing the third light) are consistent with it being a normal main sequence star, based on comparison with Yi et al. (2001) and Girardi et al. (2000) isochrones using a distance modulus $(m - M)_V = 9.72$ (Sandquist 2003). In the following analysis, we will assume that component B is a normal main sequence star and a cluster member. Based on that, we can constrain the photometric properties of the primary star in the eclipsing binary (component Aa) without resorting to models. Our calibration of the ensemble photometry (Sandquist 2003) leads to a value for the sum of the three stars of $V_{tot} = 12.729$ and $(V - I)_{tot} = 0.643$. Fig. 6 shows the VI CMD for our deconvolution of component B from the total light of the eclipsing binary. The three linked points delineate the range of $f_{Aa}(V)$ allowed by our spectra. Our derived values are $V_{bin} = 12.86 \pm 0.02$ and $(V - I)_{bin} = 0.619 \pm 0.002$.

Assuming again that the secondary component of the eclipsing binary Ab is a normal main sequence member of the cluster, we can deconvolve the (small) contribution of its light and get an estimate of the photometry of the primary alone. From the measured secondary eclipse depth and estimates of the relative flux contributions of components Aa and B, we find $I_{Ab} - I_{Aa} = 4.85$, or $I_{Ab} = 17.10^{+0.09}_{-0.08}$. Component Ab essentially does not contribute in V (only about 0.004 mag), so that the corrected primary star values are $V_{Aa} = 12.86 \pm 0.02$ and $(V - I)_{Aa} = 0.611 \pm 0.003$.

The deconvolved photometry values for the primary place it significantly to the blue of the most densely populated portions of the turnoff. We have 2152 observations of S986 in V and 816 in I and comparable numbers of observations of many other turnoff stars, so that error in the photometry relative to turnoff stars can be ruled out. If we are wrong in our assumption that component B is a normal main sequence star and it is actually an unresolved binary itself, this would make B redder and would require component Aa to be bluer still. The effective temperature measured from our spectra indicates that it is hotter than other stars that are clearly on the single-star sequence in the color-magnitude diagram.

We can compare our observations with theoretical models based on the spectroscopic

T_{eff} and $\log g$, thereby avoiding complications with color-effective temperature relations. In Fig. 5, we compare against the points that have the highest T_{eff} on the theoretical isochrones of Girardi et al. (2000; hereafter Padova) and Yi et al. (2001; hereafter Y²). Component Aa is clearly inconsistent with the turnoff points from either set of isochrones, although neither set of isochrones provides an entirely satisfactory fit to the turnoff in the color-magnitude diagram. Although the chosen amount of convective overshooting in the stellar models does affect this, comparisons of the photometry with isochrones indicates that the amount of overshooting used in the models is slightly too large for M67 (Sandquist 2003). A smaller amount of overshooting would tend to increase the difference between component Aa and the model turnoffs. However, if component Aa is a blue straggler, then its surface gravity is likely to be larger than that of a single turnoff star (which would have evolved farther from the zero-age main sequence), consistent with the observations.

4.4. Secondary Star Properties

Although component Aa does not appear to be on the single-star sequence for M67, it is quite close, and we can use that fact to constrain the properties of the fainter component Ab. An absolute comparison with theoretical models for low-mass stars is impossible because the secondary has only been detected by its eclipse in I band, data on the eclipsing binary does yet allow a complete solution of the system, and the calibrated color range for our photometry does not cover the color of component Ab. In addition, there are substantial model differences in the treatment of surface boundary conditions for low-mass models (Chabrier & Baraffe 1997), and theoretical uncertainties involving T_{eff} -color transformations (Houdashelt, Bell, & Sweigart 2000; Yi et al. 2001). In particular, there is strong evidence that models for low mass stars become too blue on the lower main sequence (von Hippel et al. 2002; Sandquist 2003).

The most direct and robust information about component Ab comes from the radius ratio R_{Ab}/R_{Aa} and the eclipse depth in I band $\Delta I = I_{Aa} - I_{Aab}$. The value of the eclipse depth, corrected for the third light contribution, is $\Delta I = 0.0124 \pm 0.0009$. Thus, any model comparisons we make have to be relative to component Aa. We used isochrones of Girardi et al. (2000) and Yi et al. (2001) to find models that were consistent with the spectroscopic T_{eff} and $\log g$ of component Aa in order to partially avoid uncertainties in T_{eff} -color transformations. These comparisons are shown in Fig. 7. The properties of component Aa are consistent with those of a star less than about 2.6 Gyr old, which can be understood if the star was formed in a collision of lower-mass stars earlier in the cluster's history.

The isochrones allow us to get an estimate of the mass and radius of component Aa using the spectroscopic gravity, although details of the distribution of the star’s chemicals introduce some uncertainty (e.g. Sills et al. 1997). This is possible because of the mass-radius relation that exists along each isochrone, with younger isochrones giving the overall largest mass and radius values. We find nearly identical ranges from both the Yi et al. (2001) and Girardi et al. (2000) isochrones: $M_{Aa} = 1.24^{+0.19}_{-0.08} M_{\odot}$ and $R_{Aa} = 1.37^{+0.24}_{-0.16} R_{\odot}$. We can also estimate the I -band magnitude of component Aa using the isochrones and the spectroscopic measurements, and again we find similar ranges from the two sets of isochrones ($M_{I,Aa} = 3.08^{+0.20}_{-0.28}$). The primary source of uncertainty in all three estimates is from the measurement of the surface gravity.

In order to make the final comparison with our observed values from the eclipse analysis, we use the models of Baraffe et al. (1998; hereafter BCAH) since they currently provide the best fit to the lower main sequence of M67 (although they begin to become too blue by $V \approx 17$; Sandquist 2003). The BCAH models are also the ones that have been most thoroughly compared to observed colors of low-mass stars, and seem to agree well down to $T_{eff} \sim 3600$ K (BCAH). The isochrones of the Y² and Padova groups employ different tables to convert from T_{eff} to color, and get widely different results. The BCAH models most nearly agree with those of the Y² or Padova groups near solar mass, where the agreement is forced by calibration to the Sun. We made a correction of 0.077 mag in I to account for zero-point differences between the Padova and Y² isochrones and those of BCAH for solar-mass models. Such a correction is justified by current uncertainties in the zero-points of T_{eff} -color relations for different sets of isochrones. Our final comparison is shown in Fig. 8. The figure indicates that component Ab is smaller and/or brighter in I band than the models predict. The uncertainties in the spectroscopic properties of component Aa mean, however, that the inconsistency is only at a little over 1σ .

A reasonable estimation of the effective temperature of star Ab is next to impossible, partly because there are not enough well-measured cool dwarf stars to set an empirical T_{eff} -color relation or calibrate a theoretical one. In addition, there is some evidence that the giant stars typically used to calibrate relations at low temperatures may follow a systematically different relation than the dwarfs (Houdashelt et al. 2000). The depth of secondary eclipse is sensitive to T_{eff} , but the interpretation *requires* the use of updated stellar atmosphere models because of strongly non-grey nature of the atmospheres of low-mass stars (e.g. Chabrier & Baraffe 1997). From the BCAH models and a distance modulus $(m - M)_I = 9.67 \pm 0.03$ (Sandquist 2003), we roughly estimate that $T_{eff} = 3700 \pm 200$ K, but we again note that this is near where their models start to diverge from color-magnitude diagrams of field dwarfs. This corresponds to a mass $M_{Ab} \sim 0.52 M_{\odot}$, so that $q \sim 0.41$.

5. Discussion and Conclusions

We have presented the first evidence of total eclipses (including eclipses of the faint secondary star in I band) in the system S986 using an extensive series of photometric observations. We have taken high-resolution spectroscopy of the system and have identified a third star that contributes to the light of the system. The third star appears to be a cluster member, but may or may not be physically associated with the eclipsing binary. The results of our analysis are given in Table 5.

The detailed analysis of our spectroscopy and photometry for the S986 indicates that the primary star in the eclipsing binary (component Aa) is a star that is slightly (but significantly) hotter than the turnoff of the cluster. Two stellar explanations for this exist. One possibility is that the primary is a normal main sequence star that is in a relatively short lived phase of its evolution. The gap in the CMD of M67 with $12.85 < V < 13.1$ corresponds to a rapid phase before and after core hydrogen exhaustion during which the central convection zone disappears and a shell fusion source is established. The size of the gap depends on exactly when the evolutionary timescale is small enough that few or no stars are likely to be found in the phase, given the total population of stars in the cluster. Several other members of M67 exist in the same portion of the CMD as component Aa (S489, S602, S610, S615, S1271, S1503, and S1575; Sandquist 2003), which may lend some credence to this idea. Because turnoff stars in clusters of M67’s age have small but significant convective cores, they put difficult constraints on the theory of convective overshooting that have not been satisfied as yet. Once they are, the CMD position of component Aa can be re-evaluated.

A second explanation is that component Aa is a blue straggler. It is somewhat difficult to piece together a scenario that can explain the system’s orbital and photometric properties, but the light curve analysis makes it clear that component Ab is a relatively normal main sequence star and that the two stars are completely detached. Component B is also consistent with being a normal main sequence star. As such, scenarios involving any kind of mass transfer to star Aa are unlikely.

Our detection of Li in component Aa is consistent with the abundances of stars on the edge of the “Li gap” (centered at $T_{eff} \approx 6700$ K). On the other hand, there has not been a detection of Li in a blue straggler in M67 to date. If component Aa was created in the merger of two stars, the detection of Li would require that the more massive star to have retained a substantial amount of surface lithium in the time before the collision, that little mass was lost from the surface of the star in the merger (see Lombardi et al. 2002 for a discussion), and the remaining Li was not substantially depleted after the merger. For a star with $T_{eff} = 6400$ K, the Li depletion timescale seems to be several Gyr (Jones et al. 1999), comparable to the age of M67, so post-merger depletion is probably not large enough

to matter here. For a star to have retained surface Li for approximately 1.5 Gyr, T_{eff} could be as low as about 5700 K based on observations of NGC 752 (Hobbs & Pilachowski 1986). This corresponds to a mass of approximately $1 M_{\odot}$, meaning that the other star involved would have had to have been low in mass ($\lesssim 0.25 M_{\odot}$). A blue straggler scenario is possible with the detection of Li, but the possible formation routes are fairly tightly constrained.

One of the most interesting details about the S986 system is that it is circularized in spite of its relatively long period and the main sequence nature of its component stars. The tidal circularization places a lower limit on the age of the binary, although the limit is not likely to be very strong given the state of our knowledge of tidal interactions (e.g. Terquem et al. 1998) and that S986 is often used to constrain the strength of tidal dissipation (after assuming an age for M67). Our best blue straggler scenario for the S986 system involves a collision of relatively low-mass stars during a close single-binary or binary-binary interaction. During the interaction two of the stars could merge to form the primary star, while a third star could be captured onto a relatively close orbit. Because strong multiple star interactions typically produce eccentric orbits, a period of circularization would still be necessary, which still should have taken most of the age of the cluster. However, this would also have the benefit of explaining why component Aa is so close to the cluster turnoff: the merger would occur before either of the stars had done much nuclear processing of their material. (If the input stars were both of low mass, this would also help.) Our isochrone comparisons imply that the merger probably happened more than 1.4 Gyr ago. Component B may or may not be associated with the creation of the system in this scenario. Long-term radial velocity monitoring would help answer that question.

Whether or not component Aa is a normal main sequence star or a blue straggler, further study of the binary is worthwhile because it provides a means of simultaneously comparing the properties of a low-mass main sequence star and a star with slightly more mass than the Sun. Because the structures of these two types of stars are rather different, theoretical models often require assumptions that can result in systematic errors when isochrones are computed. In the case of an open cluster like M67, the degree of convective core overshooting is an excellent example since it substantially affects the evolution of stars slightly more massive than the Sun (having relatively small but significant convective cores), but has negligible effect on lower main sequence models, which have surface convection zones of large extent. The surface boundary condition is also a potential source of problems because it sets the interior structure of fully- or mostly-convective stars while having a minor effect on models of stars with mass near that of the Sun (Chabrier & Baraffe 1997). M67 provides an excellent testing ground for these kinds of stellar physics issues.

E.L.S. would like to thank the director of Mount Laguna Observatory (P. Etzel) for

generous allocations of telescope time to constrain the ephemeris of this binary system, L. Detweiler for allowing us to use one of his nights to observe an eclipse, and P. Etzel and D. Latham for useful conversations. This research was supported in part by the National Science Foundation under Grant No. AST-0098696 to E.L.S.

REFERENCES

- Baraffe, I., Chabrier, G., Allard, F., & Hauschildt, P. 1998, *A&A*, 337, 403 (BCAH)
- Chabrier, G. & Baraffe, I. 1997, *A&A*, 327, 1039
- Díaz-Cordovés, J., Claret, A., & Giménez, A. 1995, *A&AS*, 110, 329
- Dinescu, D. I., Demarque, P., Guenther, D. B., & Pinsonneault, M. H. 1995, *AJ*, 109, 2090
- Edvardsson, B., Andersen, J., Gustafsson, B., Lambert, D.L., Nissen, P.E., & Tomkin, J. 1993, *A&A*, 275, 101
- Fagerholm, E. 1906, Ph.D. Thesis, Uppsala Univ.
- Fan, X. et al. 1996, *AJ*, 112, 628
- García López, R. J., Rebolo, R., & Beckman, J. E. 1988, *PASP*, 100, 1489
- Girard, T. M., Grundy, W. M., Lopez, C. E., & Van Altena, W. F. 1989, *AJ*, 98, 227
- Girardi, L., Bressan, A., Bertelli, G., & Chiosi, C. 2000, *A&AS*, 141, 371 (Padova)
- Hauschildt, P. H., Allard, F., & Baron, E. 1999, *ApJ*, 512, 377
- Honeycutt, R. K. 1992, *PASP*, 104, 435
- Hobbs, L. M. & Pilachowski, C. 1985, *ApJ*, 309, L17
- Houdashelt, M. L., Bell, R. A., & Sweigart, A. V. 2000, *AJ*, 119, 1448
- Jones, B. F., Fischer, D., & Soderblom, D. R. 1999, *AJ*, 117, 330
- Landolt, A. U. 1992, *AJ*, 104, 340
- Lombardi, J. C. Jr., Warren, J. S., Rasio, F. A., Sills, A., & Warren, A. R. 2002, *ApJ*, 568, 939
- Mathieu, R. D., Latham, D. W., & Griffin, R. F. 1990, *AJ*, 100, 1859

- Mathieu, R. D. & Latham, D. W. 1986, *AJ*, 92, 1364
- Mathieu, R. D. & Mazeh, T. 1988, *ApJ*, 326, 256
- Melo, C. H. F., Pasquini, L., & De Medeiros, J. R. 2001, *A&A*, 375, 851
- Montgomery, K. A., Marschall, L. A., & Janes, K. A. 1993, *AJ*, 106, 181
- Sanders, W. L. 1977, *A&AS*, 27, 89
- Sandquist, E. L. 2003, *MNRAS*, submitted
- Sandquist, E. L., Latham, D. W., Shetrone, M. D., & Milone, A. A. E. 2003, *AJ*, 125, 810
- Sandquist, E. L. & Shetrone, M. D. 2003, *AJ*, 125, 2173
- Shetrone, M. D. & Sandquist, E. L. 2000, *AJ*, 120, 1913
- Sills, A., Lombardi, J. C. Jr., Baily, C. D., Demarque, P., Rasio, F. A., & Shapiro, S. L. 1997, *ApJ*, 487, 290
- Stetson, P. B. 2000, *PASP*, 112, 925
- Terquem, C., Papaloizou, J. C. B., Nelson, R. P., & Lin, D. N. C. 1998, *ApJ*, 502, 788
- van den Berg, M., Orosz, J., Verbunt, F., & Stassun, K. G. 2001, *A&A*, 375, 375
- Van Hamme, W. 1993, *AJ*, 106, 2096
- von Hippel, T., Steinhauser, A., Sarajedini, A., & Deliyannis, C. P. 2002, *AJ*, 124, 1555
- Wichmann, R. 1998, *Nightfall User Manual*
- Yi, S., Demarque, P., Kim, Y.-C., Lee, Y.-W., Ree, C. H., Lejeune, T., & Barnes, S. 2001, *ApJS*, 136, 417 (Y²)
- Zhao, J. L., Tian, K. P., Pan, R. S., He, Y. P., & Shi, H. M. 1993, *A&AS*, 100, 243

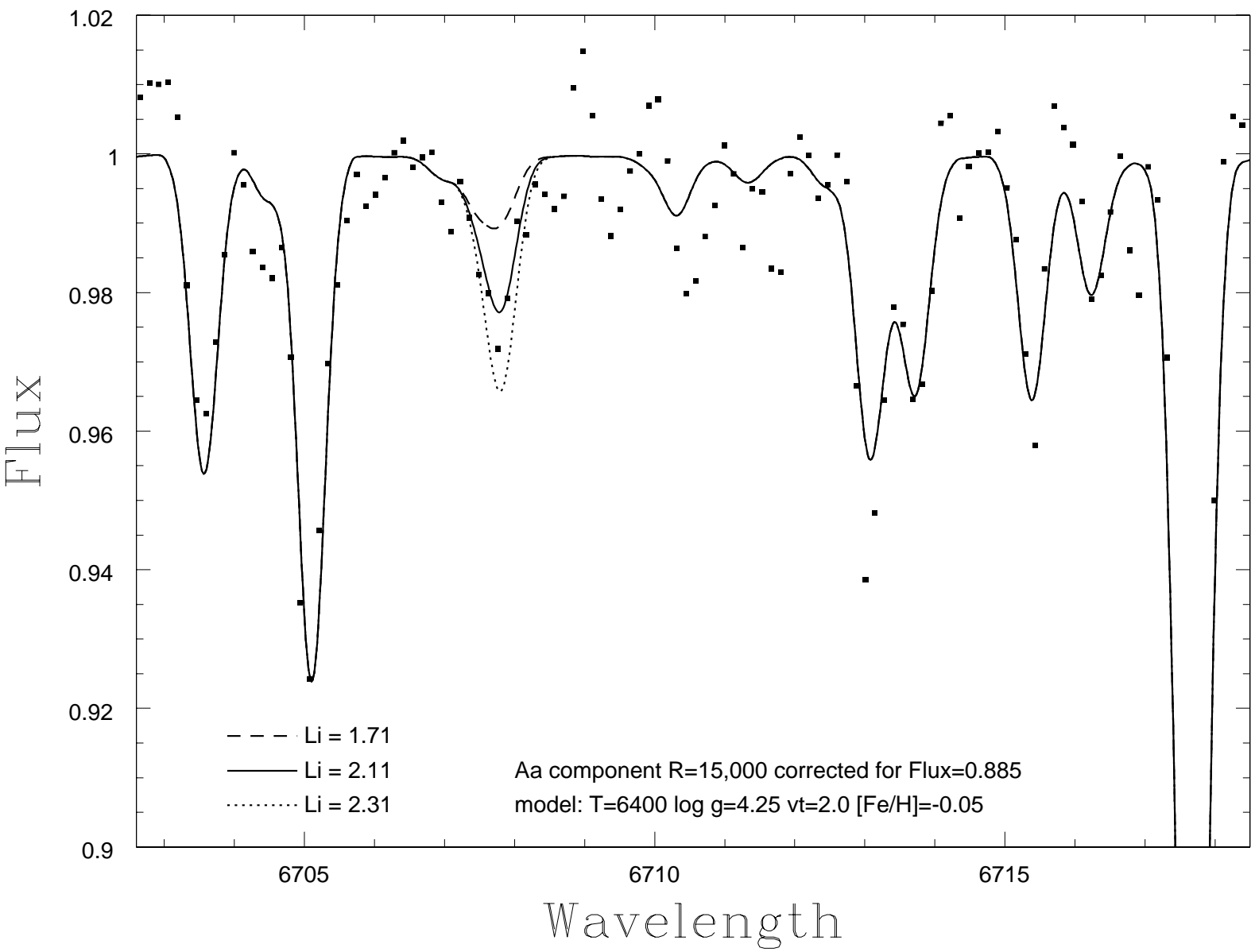


Fig. 1.— The master combined $R = 15,000$ spectrum for component Aa in the vicinity of the Li 6707 Å line, with spectral syntheses for $\log N(\text{Li}) + 12 = 1.71, 2.11$, and 2.31.

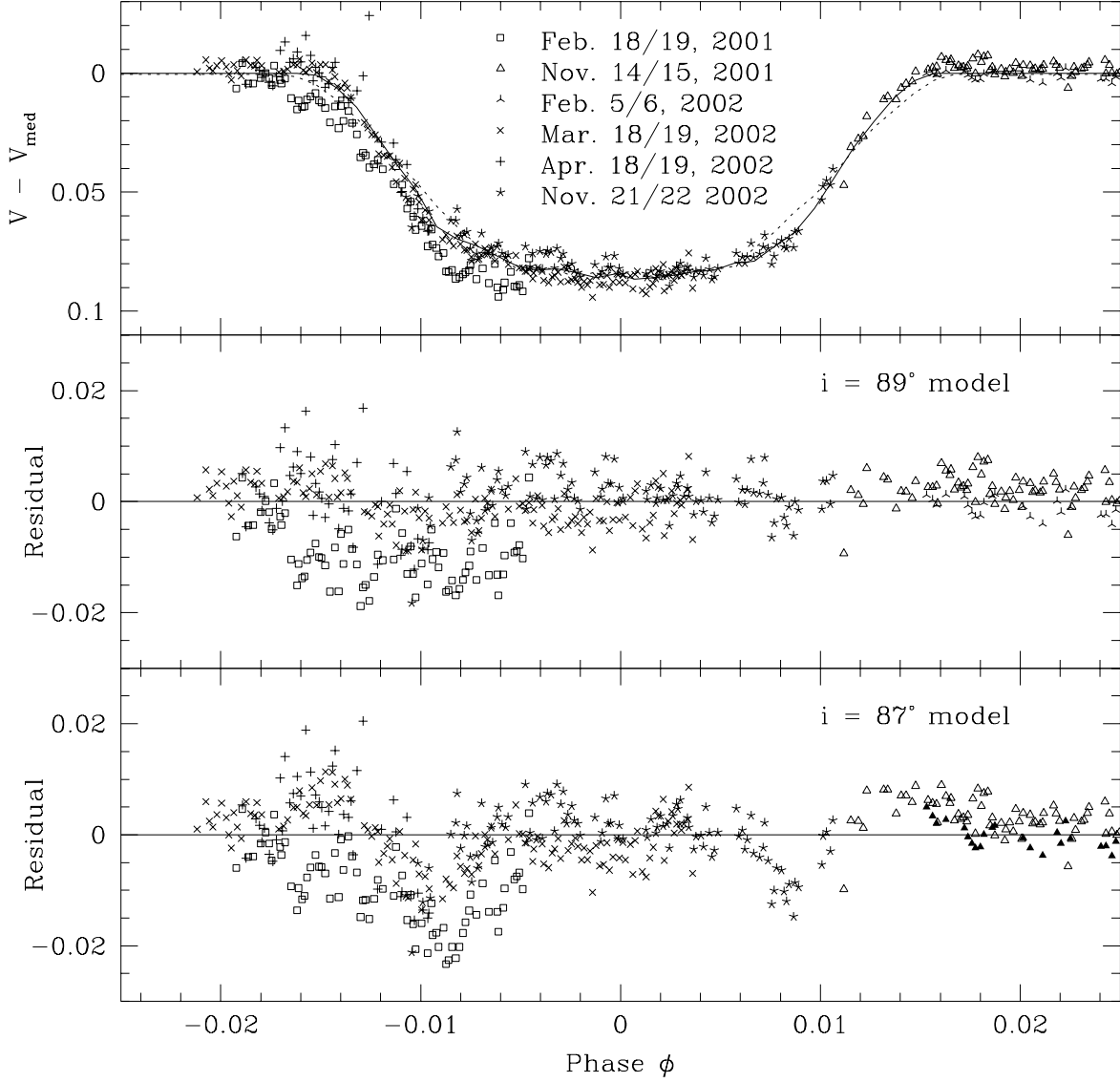


Fig. 2.— *Top panel:* V data for primary eclipse compared with best fit models assuming $i = 89^\circ$ solid line and $i = 87^\circ$ dotted line. *Bottom panels:* Residuals (in the sense of observed values minus model values) from the comparison of the observed data with models.

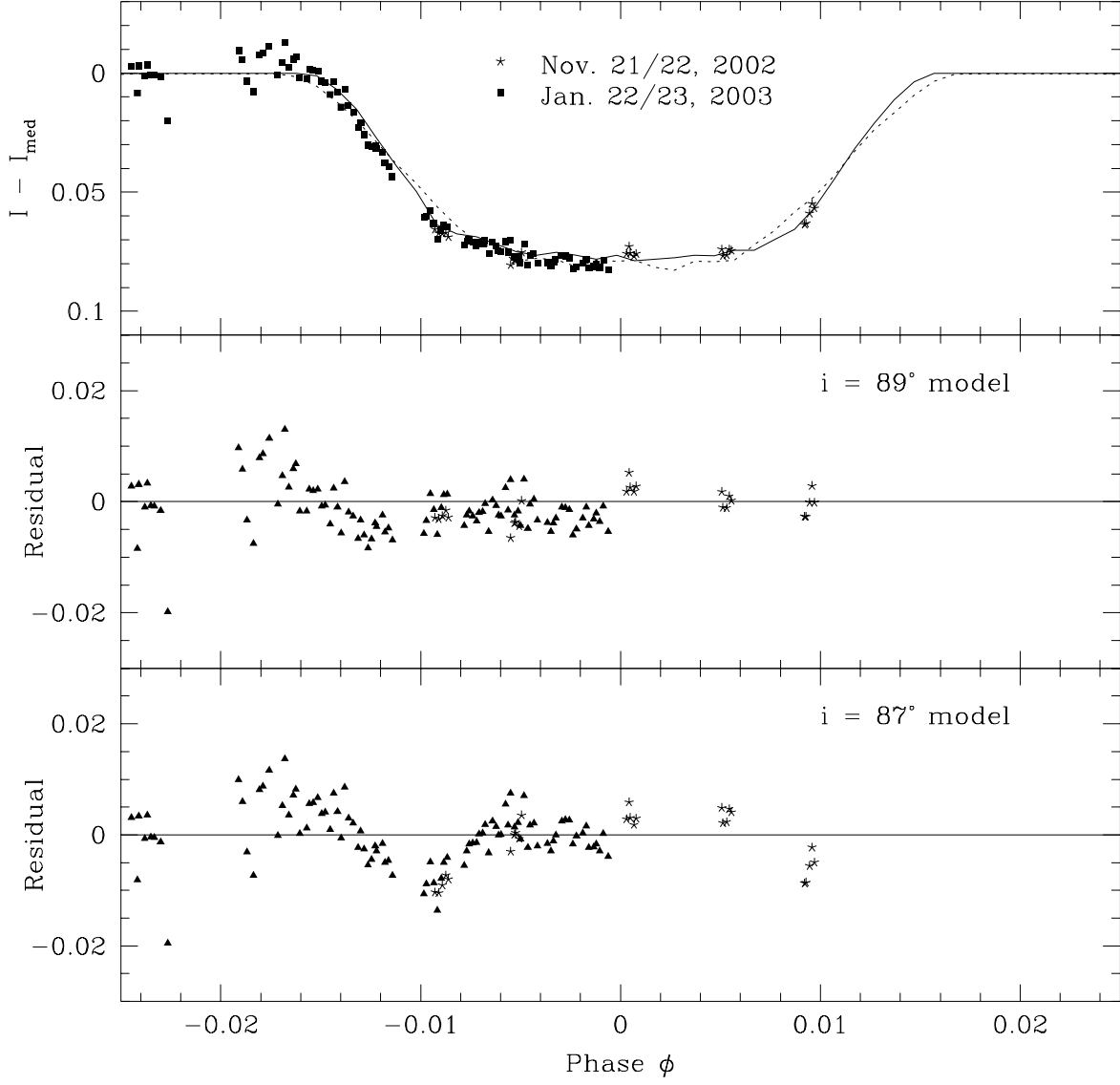


Fig. 3.— *Top panel:* I data for primary eclipse compared with best fit models assuming $i = 89^\circ$ *solid line* and $i = 87^\circ$ *dotted line*. *Bottom panels:* Residuals (in the sense of observed values minus model values) from the comparison of the observed data with models.

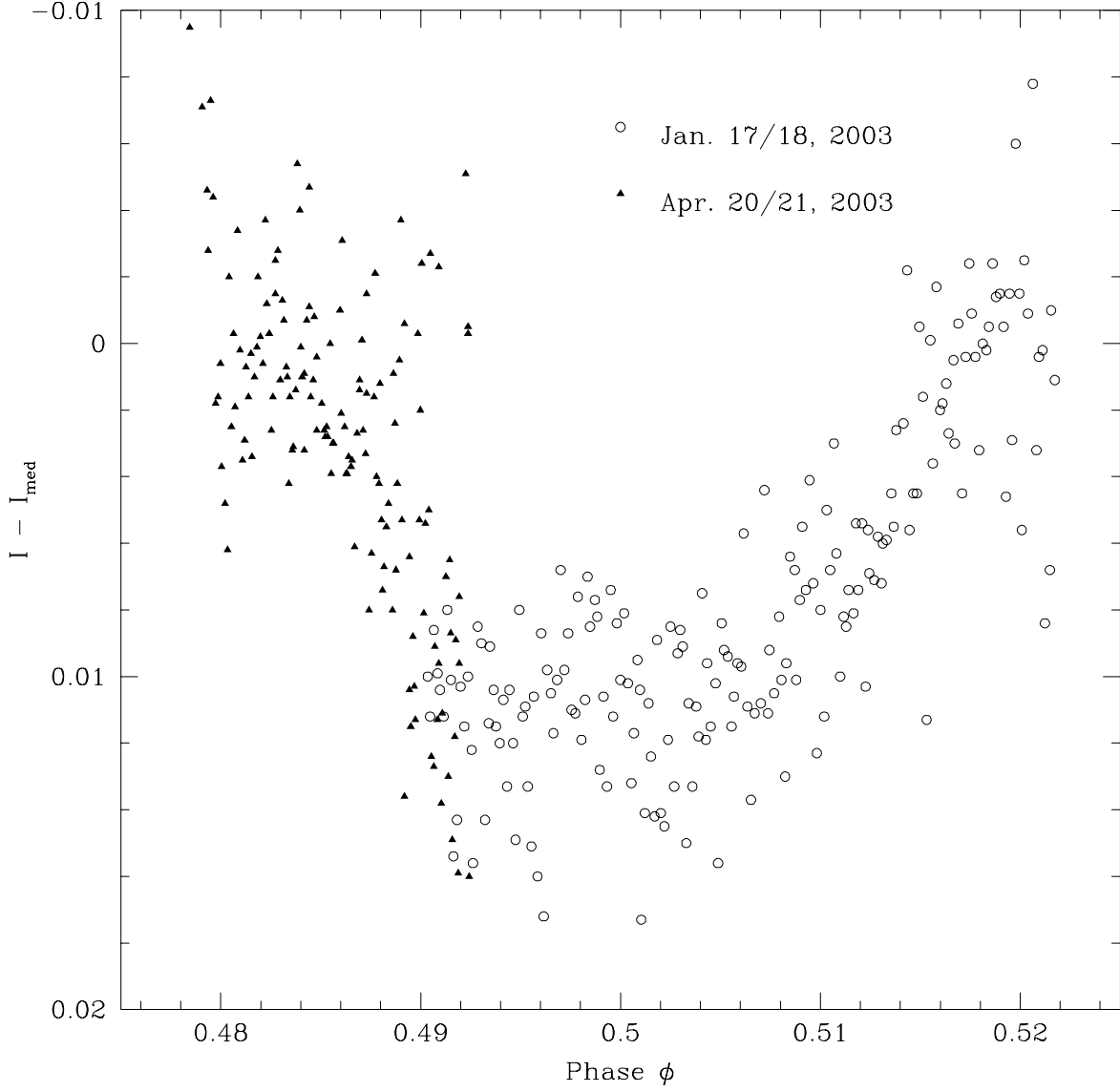


Fig. 4.— I data for secondary eclipse. The January 2003 data have been corrected for a zero point difference of 0.0025 mag.

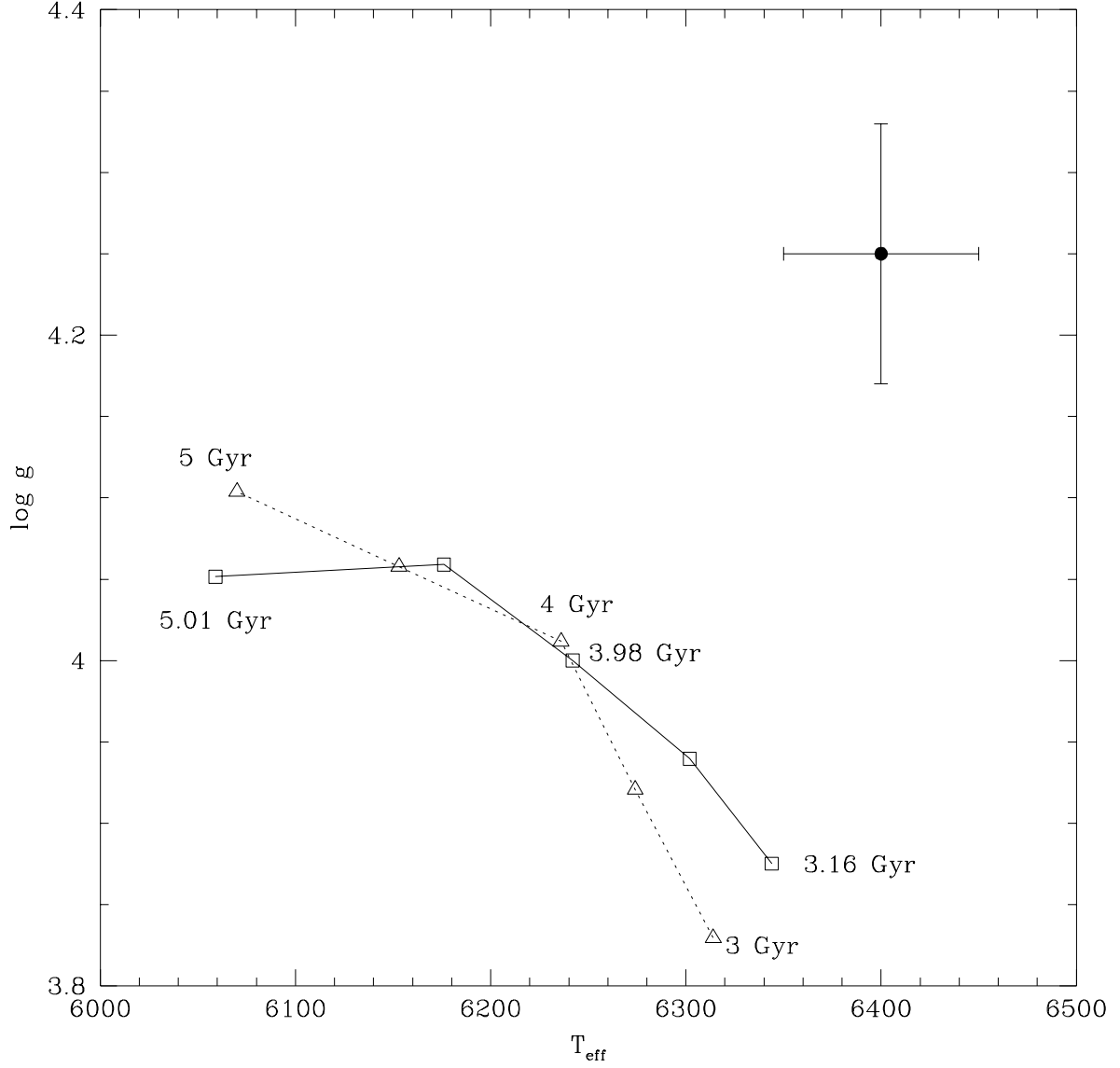


Fig. 5.— Comparison between the observed spectroscopic properties of component Aa of S986 and the turnoff points (maximum T_{eff}) from version 2 of the theoretical isochrones of Yi et al. (2001) (*dotted line, triangles*) and Girardi et al. (2000) (*solid line, squares*) with similar amounts of convective overshooting.

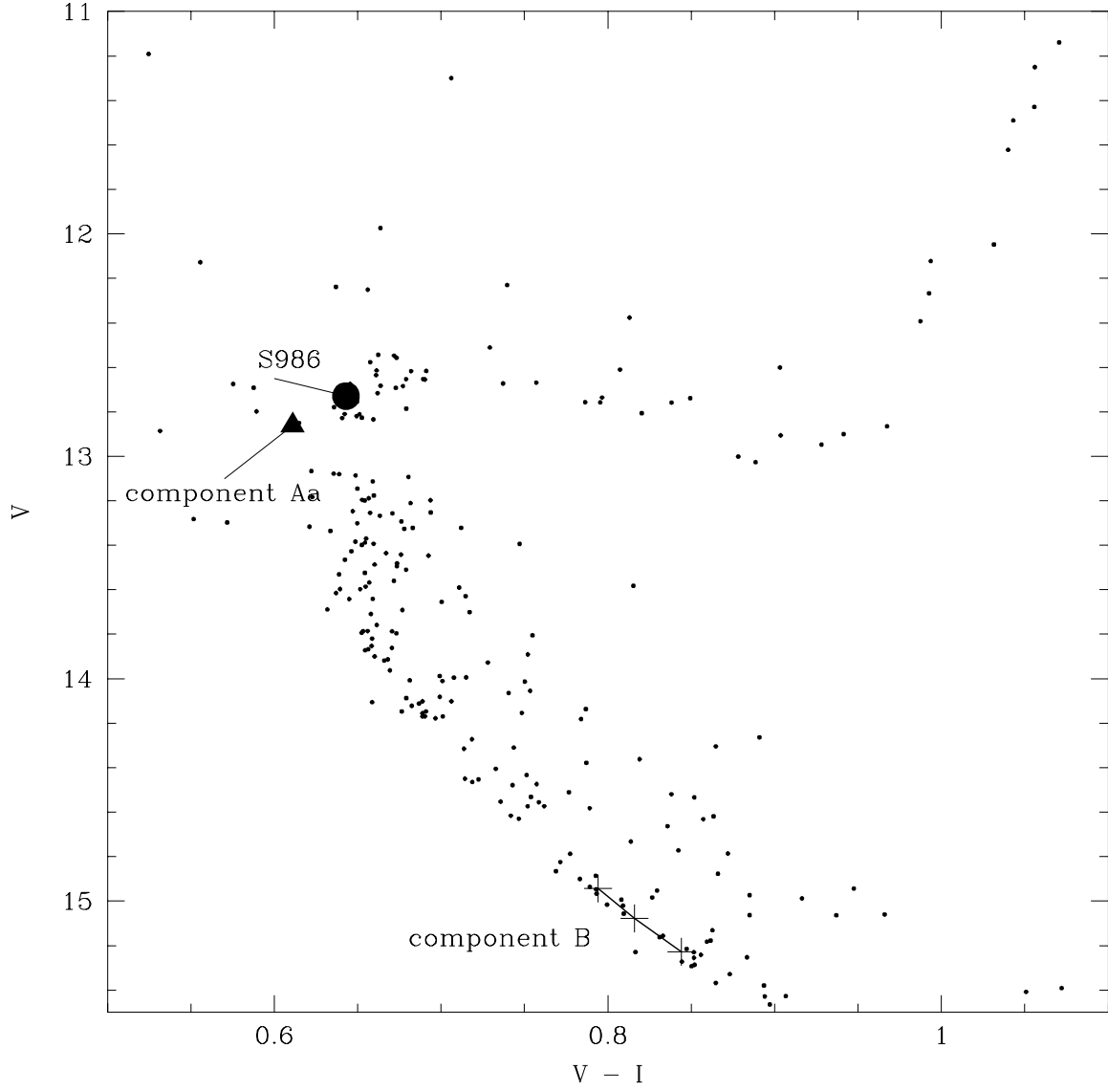


Fig. 6.— Color-magnitude diagram for the turnoff of M67. The diagram has been cleaned of non-members using the proper motions of Sanders (1977).

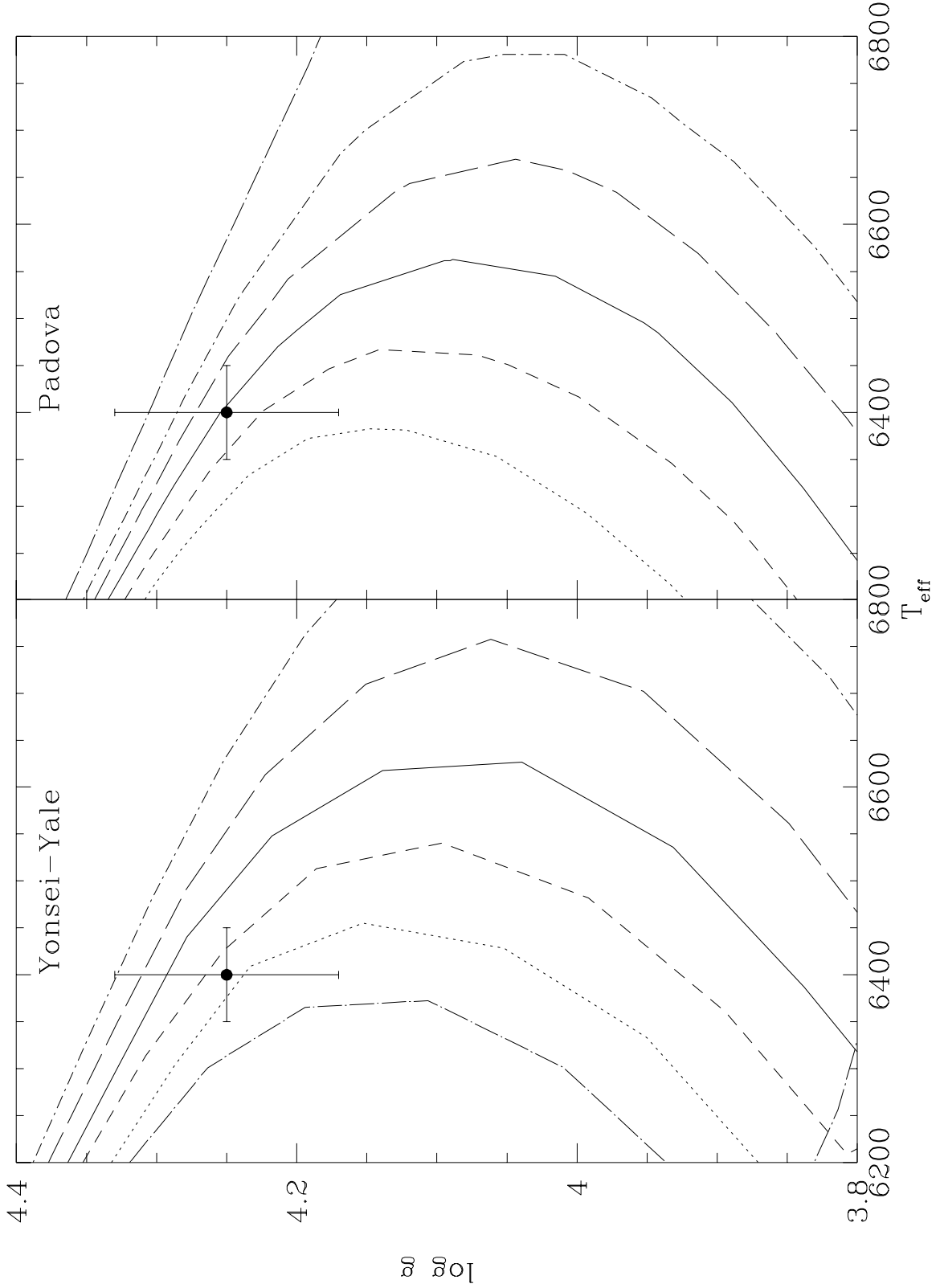


Fig. 7.— Comparison between isochrones and spectroscopic observations of component Aa (*solid circle*). From left to right, the theoretical isochrones have ages 2.75, 2.5, 2.25, 2, 1.75, 1.5, and 1.25 Gyr for Yonsei-Yale isochrones (Yi et al. 2001), and 2.512, 2.239, 1.995, 1.778,

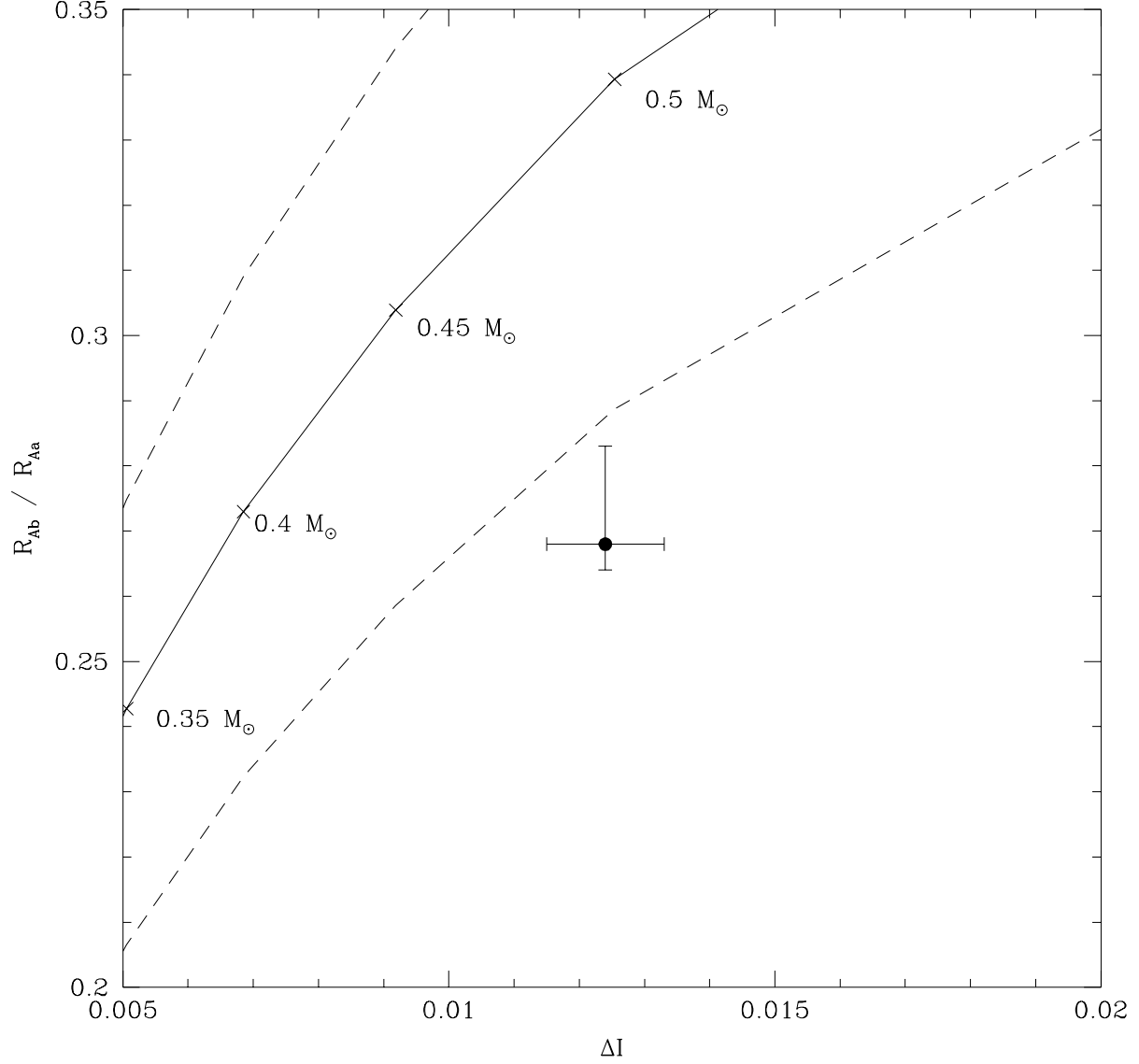


Fig. 8.— Comparison between the radius ratio R_{Ab}/R_{Aa} and secondary eclipse depth ΔI for S986. The solid circle is the observed value. Theoretical values derived from the low-mass stellar models of Baraffe et al. (1998) and the isochrones of Girardi et al. (2000) and Yi et al. (2001) are shown. The *dashed lines* show the uncertainties in the theoretical values due to uncertainties in the properties of component Aa.

Table 1. Measured Radial Velocities for Components of S986

HJD	Resolution	v_{Aa} (km s ⁻¹)	v_B (km s ⁻¹)
2452329.6377	60k	69.6 ± 0.5	36.0 ± 4.4
2452619.0219	60k	68.6 ± 0.5	35.2 ± 4.5
2452621.8263	60k	31.1 ± 0.5	
2452634.9772	60k	1.3 ± 0.5	34.1 ± 3.4
2452659.9042	60k	67.7 ± 0.4	39.6 ± 5.8
2452711.7820	15k	65.7 ± 0.3	34.6 ± 3.3
2452714.7642	15k	31.3 ± 0.4	
2452722.7410	15k	66.2 ± 0.3	34.2 ± 3.0

Table 2. Observing Log for Photometry of S986 at Mt. Laguna

#	Date	Filter	mJD Start ^a	N_{obs}
1	Dec. 5/6, 2000	<i>V</i>	1884.878	60
2	Dec. 6/7, 2000	<i>I</i>	1885.871	38
3	Dec. 7/8, 2000	<i>V</i>	1886.806	111
4	Dec. 11/12, 2000	<i>V</i>	1890.817	57
5	Dec. 12/13, 2000	<i>V</i>	1891.820	116
6	Jan. 23/24, 2001	<i>V</i>	1933.675	206
7	Jan. 25/26, 2001	<i>V</i>	1935.673	176
8	Jan. 29/30, 2001	<i>V</i>	1939.676	44
9	Jan. 30/31, 2001	<i>V</i>	1940.657	130
10	Jan. 31/Feb. 1, 2001	<i>V</i>	1941.663	161
11	Feb. 17/18, 2001	<i>V</i>	1958.655	63
12	Feb. 18/19, 2001	<i>V</i>	1959.790	75
13	Nov. 14/15, 2001	<i>V</i>	2228.901	74
14	Jan. 20/21, 2002	<i>V</i>	2295.735	91
15	Jan. 21/22, 2002	<i>V</i>	2296.687	89
16	Jan. 24/25, 2002	<i>V</i>	2299.690	124
17	Feb. 5/6, 2002	<i>V</i>	2311.649	119
18	Feb. 10/11, 2002	<i>V</i>	2316.638	167
19	Mar. 18/19, 2002	<i>V</i>	2352.625	131
20	Apr. 13/14, 2002	<i>V</i>	2378.638	103
21	Apr. 18/19, 2002	<i>V</i>	2383.661	47
22	Nov. 21/22, 2002	<i>VI</i>	2600.845	108,25
23	Jan. 17/18, 2003	<i>I</i>	2657.718	192
24	Jan. 22/23, 2003	<i>I</i>	2662.702	110
25	Feb. 17/18, 2003	<i>I</i>	2688.617	147
26	Mar. 20/21, 2003	<i>I</i>	2719.635	138
27	Apr. 20/21, 2003	<i>I</i>	2750.638	150

^amJD = HJD - 2450000

Table 3. V-Band Photometry of S986

mJD ^a	$V - V_{med}$	σ_V	Phase
1884.8806	0.0156	0.0066	0.7346
1884.9027	0.0057	0.0056	0.7367
1884.9062	−0.0056	0.0043	0.7371
1884.9095	−0.0036	0.0042	0.7374
1884.9179	−0.0056	0.0041	0.7382
1884.9198	−0.0044	0.0037	0.7384
1884.9216	−0.0004	0.0038	0.7386
1884.9231	−0.0057	0.0040	0.7387
1884.9248	0.0040	0.0038	0.7389
1884.9263	−0.0008	0.0036	0.7390
1884.9281	−0.0008	0.0047	0.7392
1884.9295	−0.0029	0.0040	0.7393
1884.9324	0.0003	0.0039	0.7396
1884.9339	−0.0019	0.0044	0.7398
1884.9354	−0.0015	0.0036	0.7399
1884.9370	−0.0014	0.0038	0.7401

^amJD = HJD - 2450000

Note. — The complete version of this table is in the electronic edition of the Journal. The printed edition contains only a sample.

Table 4. *I*-Band Photometry of S986

mJD ^a	$I - I_{med}$	σ_I	Phase
1885.8712	0.0160	0.0033	0.8304
1885.8800	0.0002	0.0033	0.8313
1885.8831	0.0041	0.0033	0.8316
1885.8847	0.0054	0.0033	0.8317
1885.8863	0.0031	0.0026	0.8319
1885.8891	0.0007	0.0033	0.8322
1885.8912	0.0006	0.0041	0.8324
1885.8926	0.0004	0.0041	0.8325
1885.8939	0.0000	0.0026	0.8326
1885.8963	0.0058	0.0033	0.8328
1885.9119	−0.0012	0.0041	0.8344
1885.9155	−0.0012	0.0033	0.8347
1885.9184	−0.0030	0.0034	0.8350
1885.9198	0.0042	0.0065	0.8351
1885.9211	−0.0166	0.0057	0.8352

^amJD = HJD - 2450000

Note. — The complete version of this table is in the electronic edition of the Journal. The printed edition contains only a sample.

Table 5. Properties of the S986 System

Parameter	Value
P (d)	10.33813 ± 0.00007
i	89_{-2}^{+1}
$[L_{Aa}/L_{tot}]_V$	0.885 ± 0.015
T_{Aa} (K)	6400 ± 50
T_{Ab} (K)	3750 ± 200
T_B (K)	5750 ± 200
V_{tot}	12.729
$(V - I)_{tot}$	0.643
V_{Aa}	12.86 ± 0.02
$(V - I)_{Aa}$	0.619 ± 0.002
V_B	15.08 ± 0.14
$(V - I)_B$	0.816 ± 0.025
I_{Ab}	17.10 ± 0.09
$(V - I)_{Ab}$	~ 2.0
$\log g_{Aa}$	4.25 ± 0.08
$v_{rot,Aa}$ (km s $^{-1}$)	< 10
$v_{rot,B}$ (km s $^{-1}$)	12 ± 4
R_{Ab}/R_{Aa}	$0.268_{-0.004}^{+0.015}$